On the sol–gel preparation of different tungstates and molybdates

A. Zalga · Z. Moravec · J. Pinkas · A. Kareiva

Abstract The preparation and characterization of the M′–M″–O nitrate–tartrate (M′ = Ca, Ba, Gd and M′ = W, Mo) precursor gels synthesized by simple, inexpensive, and environmentally benign aqueous sol–gel method is reported. The obtained gels were studied by thermal (TG/DSC) analysis. TG/DSC measurements revealed the possible decomposition pathway of synthesized M′–M″–O nitrate–tartrate gels. For the synthesis of different metal tungstates and molybdates, the precursor gels were calcined at different temperatures (650, 800, and 900 °C). According to the X-ray diffraction (XRD) analysis data, the crystalline compounds $CaMo_{1-x}W_xO_4$ doped with Ce^{3+} ions, $BaMo_{1-x}W_xO_4$ doped with Eu^{3+} ions and $Gd_2Mo_3O_{12}$ were obtained from nitrate–tartrate gels annealed at 650–900 °C temperatures. The XRD data confirmed that the fully crystalline single-phase powellite, scheelite, or $Gd_2(MoO_4)_3$ structures were formed already at 650 °C. Therefore, the suggested sol–gel method based on the complexation of metal ions with tartaric acid is suitable for the preparation of mixed tungstates–molybdates at relatively low temperature in comparison with solid-state synthesis.

Keywords Sol–gel synthesis · Precursors · TG · DSC · Tungstates · Molybdates

A. Zalga · A. Kareiva (✉)
Department of General and Inorganic Chemistry, Vilnius University, Naugarduko 24, 03225 Vilnius, Lithuania
e-mail: aivaras.kareiva@chf.vu.lt

Z. Moravec · J. Pinkas
Department of Chemistry, Masaryk Brno University, Kotlarska 2, 61137 Brno, Czech Republic

Introduction

Nowadays, considerable research attention has been devoted to trivalent lanthanide ions as luminescence centers due to the rapid development of diode lasers [1, 2]. Especially, phosphors excited by vacuum ultraviolet light have drawn a great amount of attention with their application in plasma display panels, and mercury-free fluorescent lamps [3]. Besides, the search for stable, inorganic rare-earth-based red phosphor with high absorption in the near-UV/blue spectral region is an attractive and challenging research task [4]. Moreover, nano- or micrometer-sized inorganic compounds activated by rare-earth ions have received much attention due to a wide application in luminescence devices, such as cathode ray tubes [5], field emissive display [6], and plasma display panels [7]. Such applications are highly dependent on the basic factors that govern the luminescence. For instance, particle size and morphology are primarily responsible for the luminescent properties and the device performance of Ln^{3+}-doped phosphors [8]. For practical applications, phosphors with spherical morphology of a fine size (0.5–4 μm), which could be obtained only at relatively low temperatures, may offer dual advantages over other morphologies in that they achieve high packing densities and minimize the light scattering [9].

The optical properties of trivalent rare-earth ions either in tungstates or in molybdates with scheelite ($CaWO_4$) or powellite ($CaMoO_4$) structures, respectively, have been widely investigated in the last several years [10–15]. Moreover, it is well known that rare-earth elements can form series of isomorphous molybdates with general formula $Ln_2(MoO_4)_3$, and some of these compounds show interesting fluorescence properties as well [11]. Therefore, such compounds as $CaWO_4$, $CaMoO_4$, $BaMoO_4$, and

$Gd_2Mo_3O_{12}$, which have potential industrial applications in solid-state lasers, color TV monitors, and etc. may play important role as host materials in the future technologies [10, 16–18]. Consequently, different new synthesis methods which could easily produce such kind of materials with well-determined crystallinity and controlled morphology are still very desirable.

Many different preparation techniques, such as traditional solid-state reactions [19], combustion [20], Czochralski method [21], solvothermal processes [22], microwave irradiation [23], spray pyrolysis [24], the facile microemulsion-mediated hydrothermal process [25], electrochemical [26], sonochemical [27], and sol–gel synthesis [28] are successfully used for the synthesis of different inorganic ceramic materials. Among these different synthesis routes, the solution-based synthetic methods play a crucial role in the design and production of fine ceramics and have been successful in overcoming many of the limitation of the traditional solid-state, high-temperature methods. The use of solution chemistry can eliminate major problems, such as long diffusion paths, impurities, and agglomeration, and result in products with improved homogeneity [29].

In the past few decades, many researchers have carried out the studies on the formation of metal complexes with organic ligands. Furthermore, the metal complexes with organic ligands have been used for the preparation of ceramics and metal oxide thin films by sol–gel process, using metal nitrates [30–32], chlorides [33], and acetates [34] as starting materials. Besides, metal salts are very useful, inexpensive, and very easy to handle in comparison to metal alkoxides, and hence they are good alternatives for the conversion to oxides by thermal decomposition. They can be dissolved in many kinds of organic solvents in which metal complexes are formed.

From this point of view, the wet synthesis route called an aqueous sol–gel method, is really attractive and compared to other techniques, as it has the advantages of a good control of the starting materials and of the processing parameters, a high purity of the raw materials, and the low temperature of the process. A good homogeneity of the product could be achieved by control of the stoichiometry of the starting solution.

In this article, we report the synthesis of scheelite-type $M'M''O_4$ (M' = Ba, Ca, and Gd) compounds doped with RE^{3+} ions (RE = Eu, Ce) by aqueous sol–gel synthesis route with tartaric acid as a complexing agent. Moreover, the thermal decomposition of the $M'–M''–O$ nitrate–tartrate gels (M' = Ca, Ba, Gd, Eu, Ce and M'' = W, Mo), which is the critical stage of this preparation technique was also investigated in detail. Besides, aqueous sol–gel chemistry routes based on ammonium-molybdate/tungstate as the precursor and calcium and/or barium and/or gadolinium nitrate tetrahydrates as the source of metal ions have been developed to prepare particular molybdate/tungstate powder samples doped by Eu^{3+} and Ce^{3+} ions.

Experimental details

Sample preparation

The samples of $CaMo_{1-x}W_xO_4$: 0.5% Ce (x = 0.0, 0.25, 0.5, 0.75, and 1.0), $BaMo_{1-y}W_yO_4$: z%Eu (y = 0.0, 0.5, and 1.0; z = 1, 4, and 8), and $Gd_2Mo_3O_{12}$ were prepared by an aqueous nitrate–tartrate sol–gel synthesis route. The starting materials europium oxide (Eu_2O_3, 99.99%, Alfa Aesar), gadolinium nitrate hexahydrate ($Gd(NO_3)_3 \cdot 6H_2O$, 99.99%, Sigma-Aldrich), gadolinium oxide (Gd_2O_3, 99.99%, Alfa Aesar), cerium nitrate hexahydrate ($Ce(NO_3)_3 \cdot 6H_2O$, 99.99%, Sigma-Aldrich), molybdenum oxide (MoO_3, 99.9%, Alfa Aesar), tungsten oxide (WO_3, 99.9%, Sigma-Aldrich), calcium nitrate tetrahydrate ($Ca(NO_3)_2 \cdot 4H_2O$, 99%, Alfa Aesar), barium nitrate ($Ba(NO_3)_2$, and 99.9%, Alfa Aesar) were weighed according to the desired stoichiometric ratio. Nitric acid (HNO_3 conc., Roth) and aqueous ammonia ($NH_3 \cdot 4H_2O$, conc. 26%, Sigma-Aldrich) were used as solvents and reagents to control the pH of the solutions. Tartaric acid ($C_4H_6O_6$, 99.5%, Penta) was used as a complexing agent. In the sol–gel process, MoO_3 and/or WO_3 were first dissolved in 25 mL of concentrated ammonia solution by stirring at 70–80 °C. Secondly, tartaric acid (TA) dissolved in a small amount of distilled water was added in a molar ratio of (W and/or Mo)/(TA) = 0.25, with a continuous stirring during several hours at a constant temperature. Next, the stoichiometric amount of calcium nitrate tetrahydrate, and/or barium nitrate, and/or gadolinium nitrate hexahydrate dissolved in distilled water was mixed into the reaction solution. To prevent precipitation, excess ammonia was neutralized by concentrated HNO_3 until the pH reached the value of ∼1.0. Afterward, Eu_2O_3 and/or $Ce(NO_3)_3 \cdot 6H_2O$, and/or Gd_2O_3 were added directly to the reaction mixture. Finally, the same amount of the aqueous solution of the complexing agent was repeatedly added to the reaction mixture to prevent crystallization of metal salts during the gelation process. The solution was closed with a watch glass and stirred for 60 min. The obtained clear solution was concentrated by a slow evaporation at 80 °C in an open beaker. A yellow or dark blue transparent gel formed after nearly 90% of the water has been evaporated under continuous stirring. After drying in an oven at 105 °C, fine-grained powders were obtained. The precursor xerogels were calcined for 5 h at 500 °C in alumina crucibles and reground carefully in an agate mortar. Since the gels are very combustible, slow heating (1 °C/min), especially between 150 and 300 °C, was found to be essential. After intermediate grinding, the obtained powders were repeatedly annealed in

air at ambient pressure at 650, 700, 750, 800, 900, and 950 °C, at each temperature holding for 1, 5, 10, and 30 h.

Characterization of samples

The crystallization processes of the complex precursor were examined by thermogravimetry and differential scanning calorimetry (TG–DSC, Netzsch STA 449C Jupiter instrument) using a sample weight of about 10 mg and a heating rate of 5 °C/min in flowing air (70 cm^3/min) at ambient pressure from room temperature to 1000 °C. The synthesized samples were characterized by X-ray powder diffraction analysis (D8 Bruker AXS powder diffractometer) using Cu Kα_1 radiation. The spectra were recorded at the standard rate of 1.5°2θ/min.

Results and discussion

Thermal analysis

It is well known, that thermal characterization of synthesized samples is important both for the control of the reaction process and of the properties of materials obtained. In this context, thermal analysis is a versatile group of techniques which can be used to monitor the preparative studies [35–48]. To understand pyrolysis behavior and crystallization process, the TG–DSC curves of nitrate–tartrate molecular precursors to CaMo$_{1-x}$W$_x$O$_4$ (x = 0.0, 0.25, 0.5, 0.75, and 1.0), BaMo$_{1-x}$W$_x$O$_4$ (x = 0.0, 0.5, and 1.0), and Gd$_2$Mo$_3$O$_{12}$ were recorded and they are presented in Figs. 1, 2, 3. The decomposition process in the CaMo$_{1-x}$W$_x$O$_4$ system can be roughly divided into three periods (Fig. 1, Table 1). The first weight loss starts at 136–171 °C in the TG curves and its initial part could be attributed to the removal of surface absorbed water and/or water from the coordination sphere of the metal complexes. A strong endothermic peak near 168 °C (CaMoO$_4$, Fig. 1a) and less expressed endothermic peaks around 150–155 °C (Fig. 1b–e) on the DSC curves correspond to the first period of weight loss on the TG curves. Besides, the first step of the decomposition of Ca–Mo/W–O nitrate–tartrate gel precursors could be related to the decomposition reactions of mixed-metal nitrate and ammonium salts, which starts to decompose with further increasing of temperature. The decomposition reactions of different metal salts, which have formed during gelation process as secondary crystallization phases were also suggested by weak endothermic effects near 194 °C in DSC curves, as shown in Fig. 1c and d. The exothermic peaks at 218 °C in Fig. 1b and d could be also attributed to the decomposition of ammonium nitrate, which formed by neutralization reaction between nitric acid and ammonia.
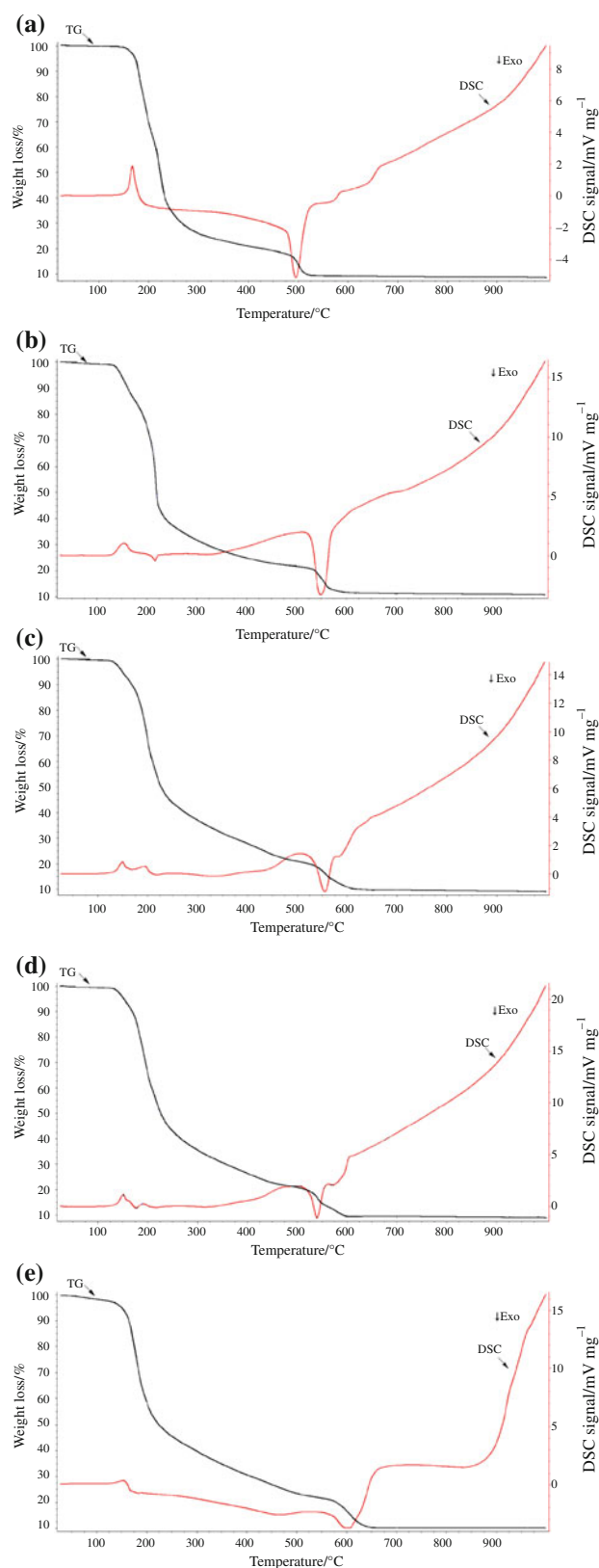
Fig. 1 Combined TG–DSC curves of the precursor gels to CaMo$_{1-x}$W$_x$O$_4$ in flowing air: CaMoO$_4$ (**a**), CaMo$_{0.75}$W$_{0.25}$O$_4$ (**b**), CaMo$_{0.5}$W$_{0.5}$O$_4$ (**c**), CaMo$_{0.25}$W$_{0.75}$O$_4$ (**d**), CaWO$_4$ (**e**)

Fig. 2 Combined TG–DSC curves of the precursor gels to BaMo$_{1-x}$W$_x$O$_4$ in flowing air: BaMoO$_4$ (**a**), BaMo$_{0.5}$W$_{0.5}$O$_4$ (**b**), BaWO$_4$ (**c**)
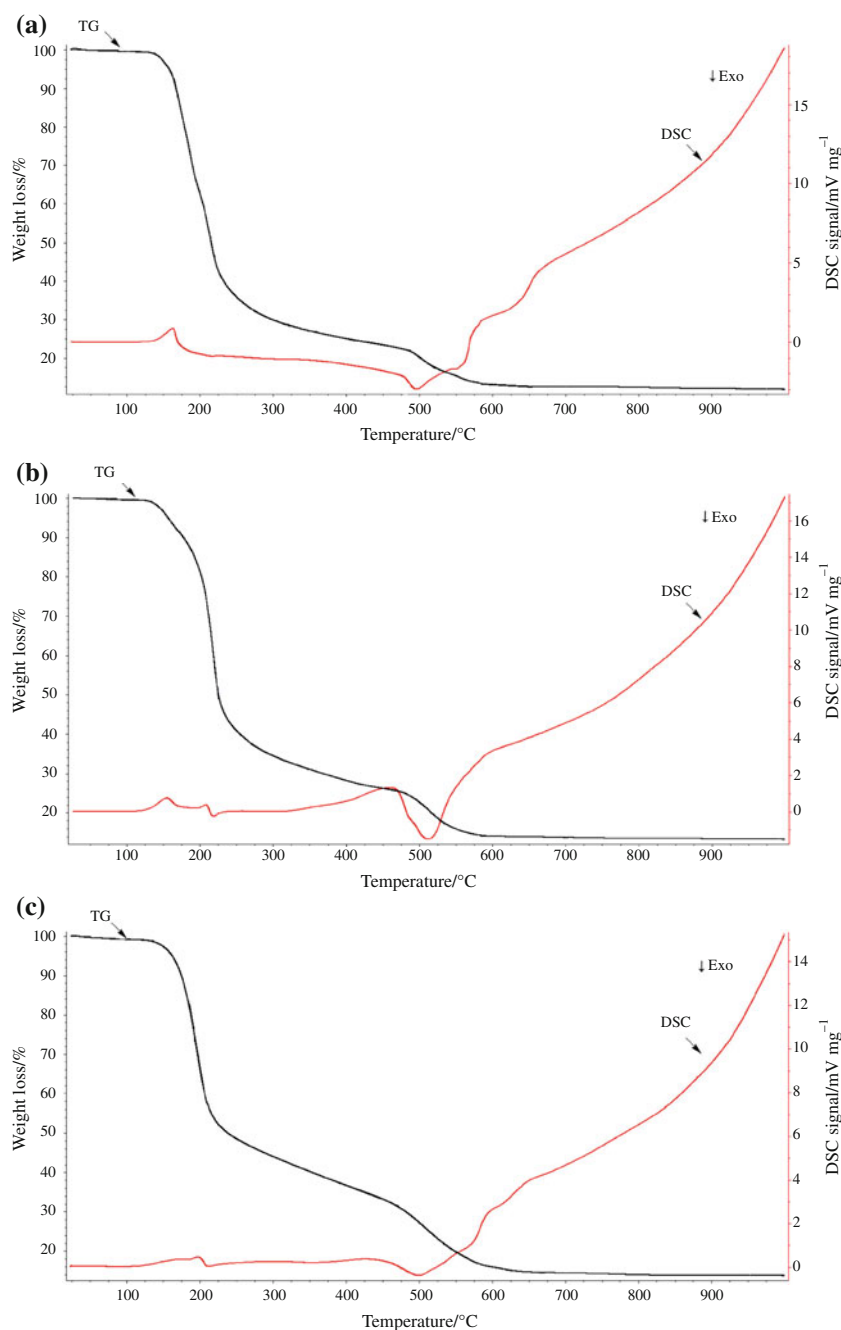

The weight loss at 400 °C is in the range 69.4–79.2%. With further increasing temperature up to 490–583 °C, the second weight loss starts (Table 1) which is attributed to the pyrolysis of the organic part of precursors. The total weight loss about 90% is indicated by the TG curves at 1000 °C. The exothermic peaks at about 496–607 °C (Table 1) are attributed to the combination of oxidation of organic groups by nitrate and air. Besides, these exothermic behaviors are closely related to further pyrolysis of intermediate products, which are usually formed during decomposition of nitrate–tartrate gel precursors. The TG curves indicate that the

weight loss of the Ca–Mo–W–O nitrate–tartrate gels caused by heating from room temperature is completed at progressively higher temperatures 530 °C (Fig. 1a), 570 °C (Fig. 1b), 600 °C (Fig. 1c, d), and 640 °C (Fig. 1e), for increasing content of W.

TG–DSC curves of the gel precursors to BaMoO$_4$, BaMo$_{0.5}$W$_{0.5}$O$_4$, and BaWO$_4$ are presented in Fig. 2. All three TG curves indicate that the weight loss of the Ba–Mo–W–O nitrate–tartrate gels occurs with the increase of temperature from room temperature to 580 °C and the decomposition process can be roughly divided into three

Fig. 3 Combined TG–DSC curves of the Gd–Mo–O precursor gels synthesized in the sol–gel process using different starting materials in flowing air: Gd(NO$_3$)$_3$·6H$_2$O (**a**) and Gd$_2$O$_3$ (**b**)
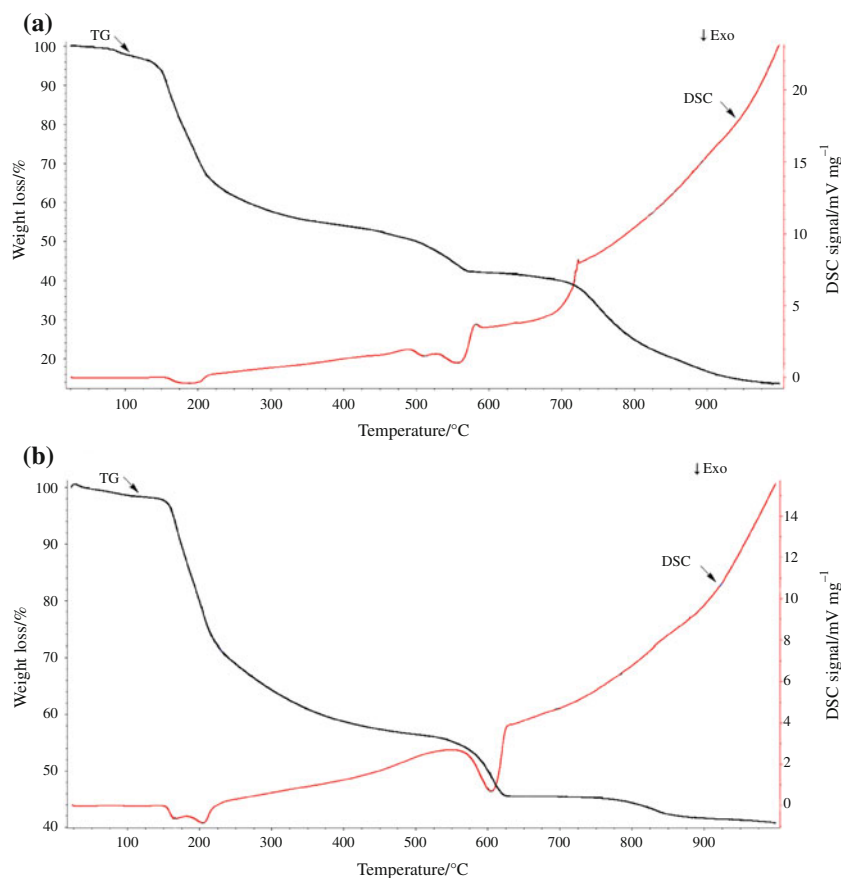
Table 1 Thermoanalytical data for the CaMo$_{1-x}$W$_x$O$_4$ gels

Precursor gel	Onset1/°C	End1/°C	Mass loss/% at 400 °C	Onset2/°C	End2/°C	Mass loss/% at 1000 °C	Endo1/°C	Exo2/°C
CaMoO$_4$	171	236	79.2	490	514	91.6	168	496
CaMo$_{0.75}$W$_{0.25}$O$_4$	139	223	75.2	537	566	89.4	155	550
CaMo$_{0.5}$W$_{0.5}$O$_4$	136	220	72.2	542	602	91.0	150	556
CaMo$_{0.25}$W$_{0.75}$O$_4$	138	220	73.7	529	599	91.3	151	540
CaWO$_4$	161	203	69.4	583	628	90.0	153	607

Table 2 Thermoanalytical data for the BaMo$_{1-x}$W$_x$O$_4$ gels

Precursor gel	Onset1/°C	End1/°C	Mass loss/% at 400 °C	Onset2/°C	End2/°C	Mass loss/% at 1000 °C	Endo1/°C	Exo2/°C
BaMoO$_4$	157	228	75.0	487	552	88.2	163	496
BaMo$_{0.5}$W$_{0.5}$O$_4$	141	229	71.8	489	539	86.8	155	512
BaWO$_4$	173	213	63.3	470	574	86.3	198	499

periods (Table 2). The first mass loss starts at temperatures 141–173 °C, corresponding to the loss of surface absorbed water and/or water from the coordination sphere of the metal complexes. The endothermic peaks at about 155–198 °C on the DSC curves show the loss of adsorbed water and ammonia from the gel. They can be also associated with the decomposition reactions of metal nitrates and ammonium salts. This process is confirmed by TG curves in Fig. 2, which show the mass losses from 63.3 to 75% occurring by 400 °C (Table 2). Further weight loss on TG curves indicates the pyrolysis process of the residual organic part of the gels. The last mass loss of about 10% is observed between 500 and 600 °C. This combustion process of residual pyrolysis products confirmed by exothermic peaks at 496 °C (Fig. 2a), 512 °C (Fig. 2b), and 499 °C (Fig. 2c), respectively. Finally, the weight remains

constant, which shows that the decomposition and combustion of all organic materials components in the precursors have been completed below 600 °C. The weak peaks on the DSC curve at ~600 and ~650 °C probably correspond to the beginning of crystallization of $BaMoO_4$, $BaMo_{0.5}W_{0.5}O_4$, and $BaWO_4$.

The TG–DSC curves of the Gd–Mo–O nitrate–tartrate gels synthesized in the sol–gel process using different starting materials either $Gd(NO_3)_3\cdot 6H_2O$, or Gd_2O_3 are shown in Fig. 3. Figure 3a and b indicates that weight loss of the precursor gels occurs in the TG curves on going from room temperature to 1000 °C, and the decomposition process can be roughly divided into four periods. The small endothermic peaks at about 150 °C (see Fig. 3a, b) on the DSC curves correspond to the first step of mass loss. The exothermic peaks at 166 °C (Fig. 3a), 198 and 205 °C (Fig. 3b) are attributed to the second weight loss step, which is associated with thermal decomposition of metal precursor. The weight loss of about 30% (Fig. 3a) and 35% (Fig. 3b) which occurs from 175 to 450 °C and from 175 to 535 °C, respectively, is attributed to the second period of thermal behavior. The third mass loss from 450 to 600 °C (see Fig. 3a) and from 535 to 625 °C (see Fig. 3b) is associated with the burning of organic parts in the pyrolysis intermediates of Gd–Mo–O nitrate–tartrate gels. The exothermic peaks at 512, 557 °C (Fig. 3a), and at 606 °C (Fig. 3b) confirm the possible combustion process of residue of mixed-metal gels. It is interesting to note, that starting from ~600 °C the TG curves for both gel precursors are quite different. The mass of Gd–Mo–O nitrate–tartrate gel prepared from $Gd(NO_3)_3\cdot 6H_2O$ decreases monotonically with increasing temperature up to 1000 °C. Surprisingly, the precursor almost completely evaporates at 1000 °C, which is very difficult to explain. The endothermic behavior on the DSC curve also is attributed to the last mass loss in the TG curve showed in Fig. 3a. Meanwhile, the last weight loss from 750 to 850 °C in the TG curve of Gd–Mo–O precursor gel obtained from Gd_2O_3 indicates the decomposition of the residuals in the gel precursor. Moreover, the observed mass loss of only about 2% from 750 to 850 °C (see Fig. 3b) indicated a possible decomposition of carbonate residuals during the crystallization process. Finally, the weight of residual Gd–Mo–O precursor gel obtained from Gd_2O_3 remains constant which indicates that the decomposition and combustion of all organic components in the precursor have been completed below 850 °C and, according to the DSC curve, the crystallization of the end product occurred. The total weight loss at 1000 °C for the $Gd(NO_3)_3\cdot 6H_2O$ and Gd_2O_3 precursors is 86.4 and 59.3%, respectively. In conclusion, the thermal decomposition of Gd–Mo–O nitrate–tartrate gels occurred in a different way depending on the source of gadolinium in the starting gel precursor.
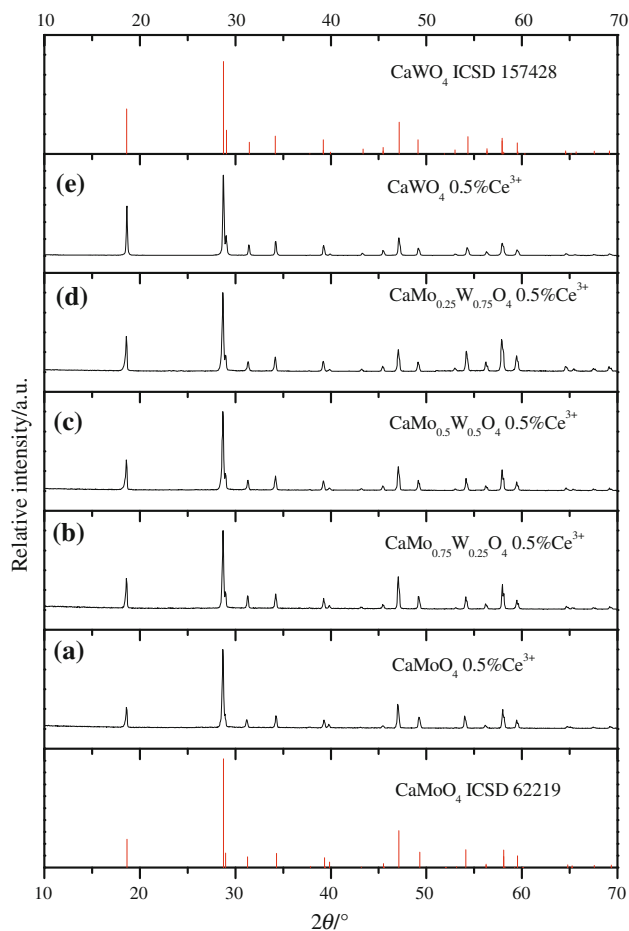
Fig. 4 XRD patterns of 0.5% Ce^{3+} ions doped $CaMo_{1-x}W_xO_4$ samples heat-treated at 800 °C for 1 h in air: **a** $CaMoO_4$, **b** $CaMo_{0.75}W_{0.25}O_4$, **c** $CaMo_{0.5}W_{0.5}O_4$, **d** $CaMo_{0.25}W_{0.75}O_4$, **e** $CaWO_4$ and standard ICSD cards of $CaMoO_4$ and $CaWO_4$
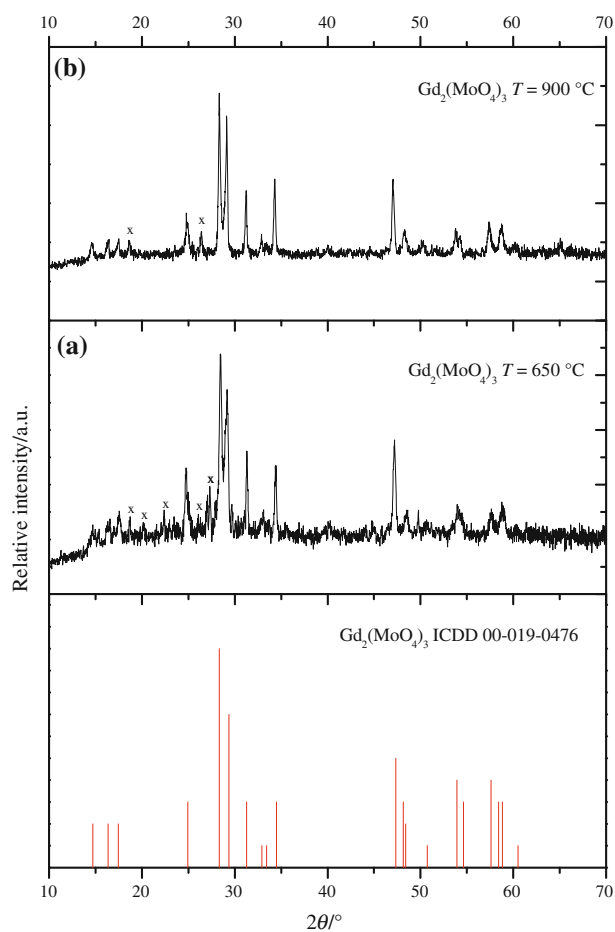
X-ray diffraction

Figure 4 exhibits powder X-ray diffraction (XRD) patterns of the $CaMo_{1-x}W_xO_4$:0.5%Ce^{3+} samples obtained by sintering the dried gels for 5 h at 500 °C and then re-annealing them for 1 h at 800 °C in air at ambient pressure. As seen from Fig. 4a and e, the calcinations of Ce–Ca–W–Mo–O nitrate–tartrate precursor gels at 800 °C produce fully crystalline $CaMoO_4$ and $CaWO_4$ phases, respectively, and no characteristic peaks due to the appearance of crystalline Ce_2O_3 (or CeO_2) phase were observed. The calcinations of Ca–Mo–O:Ce precursor gel at 800 °C for 1 h produced only the tetragonal $CaMoO_4$ phase (Fig. 4a) which corresponds to ICSD file No. 62219, and no peaks from impurities were present. Very similar situation was also observed during sol–gel preparation of calcium tungstate. In Fig. 4e only characteristic peaks of the single crystalline $CaWO_4$ compound (ICSD No. 157428) are seen. However, in the XRD pattern of the $CaMo_{0.75}W_{0.25}O_4$, $CaMo_{0.5}W_{0.5}O_4$, and $CaMo_{0.25}W_{0.75}O_4$ powders
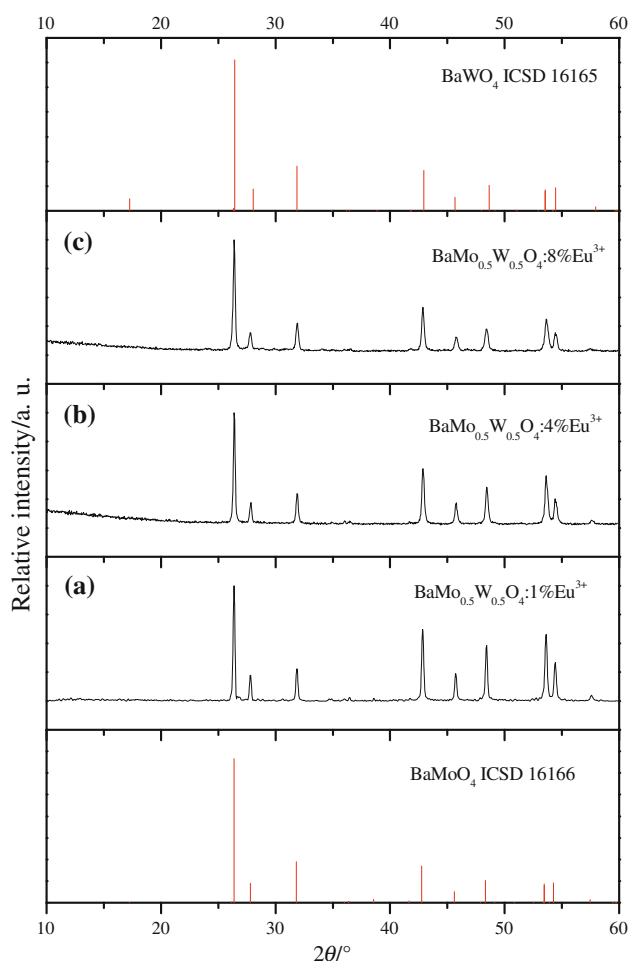
Fig. 5 XRD patterns of Eu³⁺-doped BaMo₀.₅W₀.₅O₄ precursors heat-treated at 650 °C for 5 h in air: **a** BaMo₀.₅W₀.₅O₄:1% Eu³⁺, **b** BaMo₀.₅W₀.₅O₄:4% Eu³⁺, **c** BaMo₀.₅W₀.₅O₄:8% Eu³⁺ and standard ICSD cards of BaMoO₄ and BaWO₄

Fig. 6 XRD patterns of the Gd₂Mo₃O₁₂ precursors heat-treated at 650 °C (**a**) and 900 °C (**b**) for 10 h in air using Gd(NO₃)₃·6H₂O (**a**) and Gd₂O₃ (**b**) as a starting compounds, and standard ICSD card of Gd₂Mo₃O₁₄. *x*-MoO₃

calcined at 800 °C (Fig. 4b–d, respectively) all characteristic peaks could be indexed as crystal phases of solid solutions of CaMoO₄–CaWO₄. This result clearly indicates that the crystallization of CaMo$_{1-x}$W$_x$O₄ (x = 0.0, 0.25, 0.5, 0.75, and 1.0) is entirely complete at relatively low temperature of 800 °C and is in consonant with the results of TG–DSC.

The Ba–Mo–W–O nitrate–tartrate gels were annealed at 650 °C in order to obtain single BaMoO₄ and BaWO₄ crystal phases. The XRD patterns of synthesis products are shown in Fig. 5. As seen, the calcination of Ba–Mo–W–O nitrate–tartrate precursor gels at 650 °C produced fully crystalline solid solution BaMo₀.₅W₀.₅O₄. Additionally, the samples doped with 8% of Eu³⁺ ions are also solid solution BaMo₀.₅W₀.₅O₄ (see Fig. 5c, respectively), and no peaks which could be attributed to the impurities phases in the XRD patterns were observed. These results clearly show that lanthanide dopant concentration has no influence to the crystallization of the solid solution of BaMo₀.₅W₀.₅O₄. The

results lead to the conclusion that the proposed sol–gel synthesis route is a very suitable method to prepare the single BaMoO₄ and BaWO₄ crystalline materials homogeneously doped with relatively high amount of Eu³⁺ ions.

The XRD patterns of the Gd–Mo–O nitrate–tartrate gels, synthesized using different starting gadolinium source, are presented in Fig. 6. As seen from Fig. 6a, the crystallization process of the Gd₂Mo₃O₁₂ starts at 650 °C when in the sol–gel processing MoO₃, Gd(NO₃)₃·6H₂O, and tartaric acid as a starting compounds were used. However, the large amount of impurity phases is also present in the final material. It is interesting to note, that this Gd–Mo–O precursor gel annealed even at 700 °C for 10 h showed the complete decomposition of the final inorganic residue. This result is in a good agreement with TG/DSC data presented in Fig. 3. The XRD pattern of the Gd–Mo–O gel precursor derived from gadolinium oxide and sintered at 900 °C for 30 h in air showed the crystallization of Gd₂Mo₃O₁₂ crystalline phase (Fig. 6b) and negligible amount of MoO₃ as side crystalline phase. However, the intensity of MoO₃

impurity peaks decreases significantly with increasing sintering temperature and annealing time.

Conclusions

In conclusion, a series of $CaMo_{1-x}W_xO_4$:0.5%Ce ($x = 0.0$, 0.25, 0.5, 0.75, and 1.0), $BaMo_{1-y}W_yO_4$:z%Eu ($y = 0.0, 0.5$, and 1.0, $z = 1, 4$, and 8), and $Gd_2Mo_3O_{12}$ compounds were successfully prepared by simple, inexpensive, and environmentally benign aqueous nitrate–tartrate sol–gel process. According to the XRD data, the crystallization of the Ca-MoO$_4$, CaWO$_4$, BaMoO$_4$, BaWO$_4$, and $Gd_2Mo_3O_{12}$ precursors is completed at relatively low temperatures, which is in consonant with the results of TG–DSC measurements. The crystallization of $CaMo_{0.75}W_{0.25}O_4$, $CaMo_{0.5}W_{0.5}O_4$, and $CaMo_{0.25}W_{0.75}O_4$ solid solutions was observed in the whole substitutional range. Also, we showed that these molybdates and tungstates can be easily doped with lanthanide ions without changing their crystal structure. Also, in this study we showed that the $Gd_2Mo_3O_{12}$ could be synthesized using the same sol–gel technique, however, the starting materials should be selected with care.

References

1. Wang Z, Li X, Wang G, Song M, Wei Q, Wang G, Long X. Growth and spectral properties of Tm^{3+}/Er^{3+}:NaGd(MoO$_4$)$_2$ single crystal. J Lumin. 2008;128:451–6.

2. Forster PL, Lugao AB, Brito HF, Parra DF. Calorimetric investigations of luminescent films polycarbonate (PC) doped with europium complex [Eu(TTA)$_3$(H$_2$O)$_2$]. J Therm Anal Calorim. 2009;97:497–502.

3. Gao X, Wang Y, Wang D, Liu B. Luminescent properties of $KGd_{1-x}(WO_4)_2$:Eu$_x^{3+}$ and $KGd_{1-x}(WO_4)_{2-y}(MoO_4)_y$:Eu$_x^{3+}$ phosphors in UV–VUV regions. J Lumin. 2009;129:840–3.

4. Chiu CH, Wang MF, Lee CS, Chen TM. Structural, spectroscopic and photoluminescence studies of $LiEu(WO_4)_{2-x}(MoO_4)_x$ as a near-UV convertible phosphor. Solid State Chem. 2007;180:619–27.

5. Justel T, Nikol H, Ronda C. New developments in the field of luminescent materials for lighting and displays. Angew Chem Int Ed. 1998;37:3085–103.

6. Zhou J, Gong L, Deng SZ, Chen J, She JC, Xu NS, Yang RS, Wang ZL. Growth and field-emission property of tungsten oxide nanotip arrays. Appl Phys Lett. 2005. doi:10.1063/1.2136006.

7. Zhong JP, Liang HB, Han B, Su Q, Tao Y. NaGd(PO$_3$)$_4$:Tb^{3+}— A new promising green phosphor for PDPs application. Chem Phys Lett. 2008;453:192–6.

8. Wang Z, Liang H, Wang Q, Luo L, Gong M. Luminescent properties of Tb^{3+} activated double molybdates and tungstates. Mater Sci Eng B. 2009;164:120–3.

9. Liao JS, Qiu B, Wen HR, You WX. Photoluminescence green in microspheres of CaWO$_4$:Tb^{3+} processed in conventional hydrothermal. Opt Mater. 2009;31:1513–6.

10. Lei F, Yan B. Hydrothermal synthesis and luminescence of CaMO$_4$:RE^{3+} (M = W, Mo; RE = Eu, Tb) submicro-phosphors. Solid State Chem. 2009;181:855–62.

11. Wei Q, Chen D. Luminescence properties of Eu^{3+} and Sm^{3+} coactivated Gd(III) tungstate phosphor for light-emitting diodes. Opt Laser Technol. 2009;41:783–7.

12. Fu L, Liu ZM, Liu YQ, Han BX, Wang JQ, Hu PA, Cao LC, Zhu DB. Coating carbon nanotubes with rare earth oxide multiwalled nanotubes. Adv Mater. 2004;16:350–2.

13. Tang Z, Zhou L, Wang F, Zhou L. Synthesis, characterization and luminescence study of Eu(III) tungstates and molybdates nanotubes using carbon nanotubes as templates. Spectrochim Acta. 2009;72:348–55.

14. Guo C, Zhang W, Luan L, Chen T, Cheng H, Huang D. A promising red-emitting phosphor for white light emitting diodes prepared by sol–gel method. Sensors Actuators B. 2008;133:33–9.

15. Tomaszewicz E, Dabrowska G. New cadmium and rare-earth metal molybdato-tungstates with scheelite-type structure. J Therm Anal Calorim. 2010;101:417–22.

16. Wang XX, Xian YL, Shi JX, Su Q, Gong ML. The potential red emitting $Gd_{2-y}Eu_y$ (WO$_4$)$_{3-x}$(MoO$_4$)$_x$ phosphors for UV InGaN-based light-emitting diode. Mater Sci Eng B. 2007;140:69–72.

17. Wang QM, Yan B. Hydrothermal mild synthesis of microrod crystalline Y_xGd_{2-x}(MoO$_4$)$_3$:Eu^{3+} phosphors derived from facile co-precipitation precursors. Mater Chem Phys. 2005;94:241–4.

18. Wang Z, Liang H, Zhou L, Wu H, Gong M, Su Q. Luminescence of $(Li_{0.333}Na_{0.334}K_{0.333})$Eu(MoO$_4$)$_2$ and its application in near UV InGaN-based light-emitting diode. Chem Phys Lett. 2005;412:313–6.

19. Marques APA, Longo VM, Melo DMA, Pizani PS, Leite ER, Varela JA, Longo E. Shape controlled synthesis of CaMoO$_4$ thin films and their photoluminescence property. J Solid State Chem. 2008;181:1249–57.

20. Yang P, Yao GQ, Lin JH. Photoluminescence and combustion synthesis of CaMoO$_4$ doped with Pb^{2+}. Inorg Chem Commun. 2004;7:389–91.

21. Jia GH, Tu CY, You ZY, Li JF, Zhu ZJ, Wang Y, Wu BC. Czochralski technique growth of pure and rare-earth-doped SrWO$_4$ crystals. J Cryst Growth. 2004;273:220–5.

22. Byun HJ, Song WS, Kim YS, Yang H. Solvothermally grown Ce^{3+}-doped $Y_3Al_5O_{12}$ colloidal nanocrystals: spectral variations and white LED characteristics. J Phys D Appl Phys. 2010. doi:10.1088/0022-3727/43/19/195401.

23. Thongtem T, Kaowphong S, Thongtem S. Influence of cetyltrimethylammonium bromide on the morphology of AWO$_4$ (A = Ca, Sr) prepared by cyclic microwave irradiation. Appl Surf Sci. 2008;254:7765–9.

24. Sivakumar R, Raj A, Subramanian B, Jayachandran M, Trivedi DC, Sanjeeviraja C. Preparation and characterization of spray deposited n-type WO$_3$ thin films for electrochromic devices. Mater Res Bull. 2004;39:1479–89.

25. Gong Q, Li G, Qian X, Cao H, Du W, Ma X. Synthesis of single crystal CdMoO$_4$ octahedral microparticles via microemulsion-mediated route. Colloid J Interface Sci. 2006;304:408–12.

26. Sun Y, Ma J, Jiang X, Fang J, Song Z, Gao C, Liu Z. Ethylene glycol-assisted electrochemical synthesis of CaMoO$_4$ crystallites with different morphology and their luminescent properties. Solid State Sci. 2010;12:1283–6.

27. Phuruangrat A, Thongtem T, Thongtem S. Analysis of lead molybdate and lead tungstate synthesized by a sonochemical method. Curr Appl Phys. 2010;10:342–5.

28. Mackenzie JD, Bescher EP. Chemical routes in the synthesis of nanomaterials using the sol–gel process. Acc Chem Res. 2007;40:810–8.

29. Parhi P, Karthik TN, Manivannan V. Synthesis and characterization of metal tungstates by novel solid-state metathetic approach. J Alloys Compd. 2008;465:380–6.

30. Zalga A, Beganskiene A, Kareiva A. Sol-gel synthesis and superconducting properties of Bi-2212 high-T_C superconductors. Polish J Chem. 2007;81:1547–53.

31. Predoana L, Malic B, Zaharescu M. $LaCoO_3$ formation from precursors obtained by water-based sol–gel method with citric acid. J Therm Anal Calorim. 2009;98:361–6.

32. Waqas H, Qureshi AH. Low temperature sintering study of nanosized Mn-Zn ferrites synthesized by sol-gel auto combustion process. J Therm Anal Calorim. 2010;100:529–35.

33. Zalga A, Reklaitis J, Norkus E, Beganskiene A, Kareiva A. A comparative study of $YBa_2Cu_4O_8$ (Y-124) superconductors prepared by a sol–gel method. Chem Phys. 2006;327:220–8.

34. Kodaira CA, Brito HF, Felinto MCFC. Luminescence investigation of Eu^{3+} ion in the $RE_2(WO_4)_3$ matrix (RE = La and Gd) produced using the Pechini method. J Solid State Chem. 2003;171: 401–7.

35. Kareiva A, Karppinen M, Niinistö L. Sol-gel synthesis of superconducting $YBa_2Cu_4O_8$ using acetate and tartrate precursors. J Mater Chem. 1994;4:1267–70.

36. Madarasz J, Leskelä T, Rautanen J, Niinistö L. Oxidation of alkaline-earth-metal sulfide powders and thin films. J Mater Chem. 1996;6:781–7.

37. Karppinen M, Niinistö L, Yamauchi H. Studies on the oxygen stoichiometry in superconducting cuprates by thermoanalytical methods. J Therm Anal Calorim. 1997;48:1123–41.

38. Madarasz J, Leskelä T, Pokol G, Niinistö L. Thermally induced changes in the oxidation state of cerium(IV). A study of carbonate and chloro complexes. J Therm Anal Calorim. 1997;49: 1347–55.

39. Kareiva A. A thermogravimetric study of the stability and reduction of the precursors for mercury-based superconductors. Thermochim Acta. 1997;298:155–9.

40. Van Bael MK, Kareiva A, Vanhoyland G, Mullens J, Franco D, Yperman J, Van Poucke LC. Influence of calcium substitution on the formation and thermal stability of the $YBa_2Cu_4O_8$ superconductor. Thermochim Acta. 1999;340–341:407–16.

41. Tautkus S, Kazlauskas R, Kareiva A. Thermogravimetric analysis—a powerful tool for the refinement of the synthesis process of Hg-based superconductors. Talanta. 2000;52:189–99.

42. Krunks M, Madarasz J, Leskelä T, Mere A, Niinistö L, Pokol G. Study of zinc thiocarbamide chloride, a single-source precursor for zinc sulfide thin films by spray pyrolysis. J Therm Anal Calorim. 2003;72:497–506.

43. Nenartaviciene G, Tonsuaadu K, Jasaitis D, Beganskiene A, Kareiva A. Preparation and characterization of superconducting $YBa_2(Cu_{1-x}Cr_x)_4O_8$ oxides by thermal analysis. J Therm Anal Calorim. 2007;90:173–8.

44. Acik IO, Madarasz J, Krunks M, Tonsuaadu K, Pokol G, Niinistö L. Titanium(IV) acetylacetonate xerogels for processing titania films. A thermoanalytical study. J Therm Anal Calorim. 2009;97: 39–45.

45. Navarro MC, Lagarrigue MC, De Paoli JM, Carbonio RE, Gomez MI. A new method of synthesis of $BiFeO_3$ prepared by thermal decomposition of $Bi[Fe(CN)_6] \cdot 4H_2O$. J Therm Anal Calorim. 2010;102:655–60.

46. Varga PP, Madarasz J, Pokol G. Evolved gas analysis in modelling studies of pre-sintering step in fabrication of ceramic alumina specimens. J Anal Appl Pyrol. 2010;87:231–5.

47. Frost RL, Palmer SJ, Grand L-M. Synthesis and thermal analysis of indium-based hydrotalcites of formula $Mg_6In_2(CO_3)(OH)_{16} \cdot 4H_2O$. J Therm Anal Calorim. 2010;101:859–63.

48. Malghe YS. Nanosized $SrTiO_3$ powder from oxalate precursor microwave aided synthesis and thermal characterization. J Therm Anal Calorim. 2010;102:831–6.